Journal of Applied Physics | ARTICLE | scitation.org/journal/jap

Symmetry-enforced planar nodal chain phonons in non-symmorphic materials

Cite as: J. Appl. Phys. 132, 224401 (2022); doi: 10.1063/5.0129290
Submitted: 7 October 2022 · Accepted: 16 November 2022 ·
Published Online: 8 December 2022

View Online Export Citation CrossMark

Hong-Ao Yang, Hao-Yu Wei, and Bing-Yang Cao[a)]

AFFILIATIONS

Key Laboratory for Thermal Science and Power Engineering of Ministry of Education, Department of Engineering Mechanics, Tsinghua University, Beijing 100084, China

[a)]Author to whom correspondence should be addressed: caoby@tsinghua.edu.cn. Tel./Fax: +86-10-6279-4531

ABSTRACT

Nodal chains in which two nodal rings connect at one point were recently discovered in non-symmorphic electronic systems and then generalized to symmorphic phononic systems. In this work, we identify a new class of planar nodal chains in non-symmorphic phononic systems, where the connecting rings lie in the same plane. The constituting nodal rings are protected by mirror symmetry, and their intersection is guaranteed by the combination of time-reversal and non-symmorphic twofold screw symmetry. The connecting points are fourfold degenerate while those in previous works are twofold degenerate. We found 8 out of 230 space groups that can host the proposed planar nodal chain phonons. Taking wurtzite GaN (space group No. 186) as an example, the planar nodal chain is confirmed by first-principles calculations. The planar nodal chains result in two distinct classes of drumhead surface states on the [10(–1)0] and the [0001] surface Brillouin zones. Our finding reveals a class of planar nodal chains in non-symmorphic phononic systems, expanding the catalog of topological nodal chains and enriching the family of topological surface states.

I. INTRODUCTION

Topological quantum states attract much attention in condensed matter physics nowadays since they delineate quantum phase transition upon the change of topological invariants.[1–5] In the last decade, topological semimetal states, in which the low energy excitations near band degenerate points can be described by relativistic Dirac and Weyl equations, were found in 3D solids.[6–9] Weyl and Dirac points are one zero-dimensional band degeneracies in k space. Moreover, higher dimensional degeneracies like nodal lines,[10–13] nodal chains,[14] nodal knots,[15] and nodal surfaces[16,17] were classified in the presence of lattice symmetries. The symmetry constraints of lattices are essential for band degeneracies of dimensions higher than zero. For example, a twofold band degenerate point can exist without lattice symmetry, while a twofold band degenerate line preserves under the protection of mirror symmetry in the simplest case. However, considering numerous lattice symmetries in all 230 space groups, the high-dimensional band degeneracies are still in short supply, especially in phononic systems.

Phonons, as another elementary excitation in solids, can also display nontrivial degeneracy and topological effects. Phonons play an important role in heat transport, electron–phonon energy transfer, and superconductivity. The analog of semimetal states in phonons is not restricted by the Fermi level since the entire frequency range of phonons can be excited and observed in experiments, significantly enriching potential topological phononic materials. Due to the absence of the spin degree of freedom and Kramers degeneracy, nontrivial semimetal states in phononic systems are mostly Weyl states. According to the dimension of degeneracy, they can be divided into 0-D Weyl points,[18–20] 1-D Weyl nodal lines,[21–25] and 2-D Weyl nodal surfaces.[26–29] Recently, phononic nodal lines of different shapes were reported, including helical nodal lines,[21] straight nodal lines,[22,23] and nodal rings.[24,25,30,31] Taking more symmetry constraints into consideration, nodal rings were found to build up chain-like geometries.[14,32]

Nodal chains formed by intersecting nodal rings from different planes were discovered in electronic systems in the first place,[14] where the intersection is guaranteed by non-symmorphic symmetries and is immune to spin–orbit coupling. The concept of nodal chains was soon after introduced to phononic systems,[30,32] whereas the intersection is protected by symmorphic symmetries. However, it remains unclear whether non-symmorphic symmetry-protected nodal chains can exist in phononic systems, which is critical given the fact that non-symmorphic space groups count up to 157 out of 230 space groups. In addition, currently known nodal chains are built from nodal rings in different planes, while nodal chains composed of nodal rings lying in one plane are still missing.

Given the fact that phonons cannot directly couple to electromagnetic fields, the observation and manipulation of topological behaviors in phononic systems are challenging. The existence of bulk topological phononic states has been confirmed by measuring phonon dispersion with inelastic x-ray scattering experiments,[33] while topological surface phonon states are currently unachievable due to the lack of experimental techniques. However, the calculation of the surface density of states and results of molecular dynamics simulations[34] have shown the presence of surface phonon states, consistent with theoretical predictions. Another approach is observing topological effects in designed mechanical systems. Pseudospins and time-reversal breaking can be introduced to mechanical systems, enriching their topological effects. Quantum spin Hall-like effects,[35] phononic waveguide,[36] and phononic logic[37] are found in artificial mechanical systems. Considering the difficulty in experiments, theoretical predictions and calculations are essential in finding new topological phonon materials.

In this work, we identify a new class of planar nodal chains protected by non-symmorphic symmetries in phononic systems. The constituting nodal rings lie in the same mirror-invariant plane, thus named planar nodal chains. Their intersection point is a fourfold degenerate point that is protected from gapping by a combination of time-reversal symmetry and non-symmorphic screw symmetry. The symmetry conditions do not apply to electronic systems due to the spin degree of freedom. We identified eight space groups that can host the planar nodal chain phonons, including known realistic materials. Based on first-principles calculations, we demonstrated the existence of planar nodal chain phonons in a representative material, wurtzite GaN. In addition, the planar nodal chain leads to arc states both on surface Brillouin zones oblique to the mirror plane and perpendicular to the mirror plane, facilitating experimental verification.

II. SYMMETRY CONSTRAINTS

Nodal rings are one-dimensional degeneracies in three-dimensional momentum space. The codimension is two, so extra crystal symmetries are needed to stabilize the nodal lines (rings). One of them is mirror symmetry $\mathsf{M}_x:(x, y, z, t) \mapsto (-x, y, z, t)$. Here, we take $x = 0$ as the mirror-invariant plane. In phonon systems without the spin degree of freedom, $\mathsf{M}_x^2 = 1$, and the eigenvalues of M_x are ± 1. Eigenstates with opposite mirror eigenvalues are forbidden to hybridize, enabling twofold band degeneracy, that is, the nodal ring, as shown in Fig. 1(a). We refer to the degenerate states as $|f_+\rangle$ and $|f_-\rangle$, where the subscripts denote mirror eigenvalues. Introducing more symmetry, the band degeneracy can expand to fourfold at certain points, as explained below.

A combination of time-reversal symmetry T and twofold screw symmetry S_z guarantees Kramers degeneracy in the $k_z = \pi$ plane in spinless systems, forming nodal surfaces.[16] We demonstrate as follows that T, S_z, and M_x together generate two sets of twofold irreducible representations in the $(k_x = 0,\ k_z = \pi)$ high symmetry line and further lead to a fourfold degenerate point. In real space, T and S_z act as

$$\mathsf{T}:(x, y, z, t) \mapsto (x, y, z, -t),$$
$$\mathsf{S}_z:(x, y, z, t) \mapsto \left(-x, -y, z + \frac{1}{2}, t\right), \tag{1}$$

while in momentum space,

$$\mathsf{T}:(k_x, k_y, k_z) \mapsto (-k_x, -k_y, -k_z),$$
$$\mathsf{S}_z:(k_x, k_y, k_z) \mapsto (-k_x, -k_y, k_z). \tag{2}$$

We have $[\mathsf{T}, \mathsf{S}_z] = 0$, and the combined symmetry $\mathsf{S} = \mathsf{T}\mathsf{S}_z$ acts as

$$\mathsf{S}:(x, y, z, t) \mapsto \left(-x, -y, z + \frac{1}{2}, -t\right),$$
$$(k_x, k_y, k_z) \mapsto (k_x, k_y, -k_z). \tag{3}$$

Notice that S_z^2 is equal to a translation along the z axis by a lattice constant, so we have $\mathsf{S}^2 = \mathsf{S}_z^2 = -1$ when $k_z = \pi$. Meanwhile, S preserves k vector since $k_z = \pi$ is equivalent to $k_z = -\pi$. So, S ensures Kramers degeneracy in the $k_z = \pi$ plane, making all representations twofold irreducible. Adding this condition to the mirror plane where $k_x = 0$, $|f_+\rangle$ and $|f_-\rangle$ are

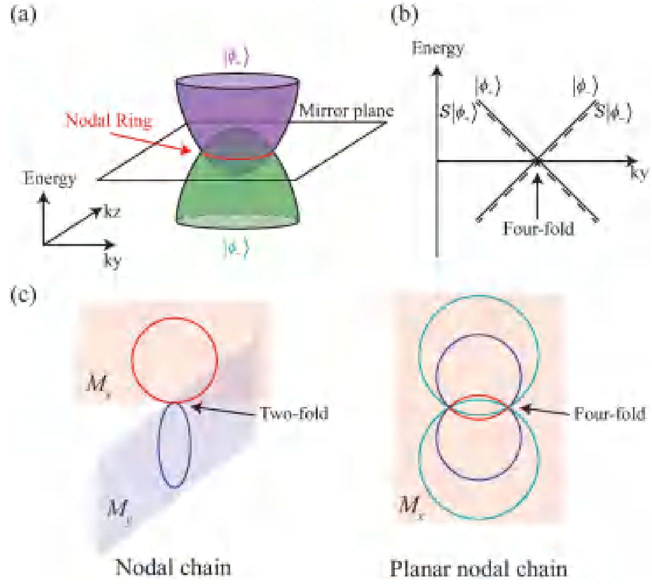

FIG. 1. (a) Sketch of the nodal ring formed on the mirror plane where $k_x = 0$. $|f_+\rangle$ and $|f_-\rangle$ are forbidden to hybridize. (b) Four orthogonal states $|f_+\rangle$, $|f_-\rangle$, $\mathsf{S}|f_+\rangle$, and $\mathsf{S}|f_-\rangle$ generating a fourfold degenerate point in the $(k_x = 0,\ k_z = \pi)$ high symmetry line. (c) Illustration of the nodal chain[14,32] and the planar nodal chain (this work). M_x and M_y denote mirror planes. Solid lines denote nodal rings.

inseparable from the other two states, $S|f_+\rangle$ and $S|f_-\rangle$. The following four states are forbidden from hybridization along the high symmetry line ($k_x = 0,\ k_z = \pi$):

$$|f_+\rangle,\ |f_-\rangle, S|f_+\rangle, S|f_-\rangle:$$

To prove their orthogonality, we take $|f_+\rangle$ as an example. $|f_+\rangle$ and $S|f_+\rangle$ are Kramers pairs, so they are immune from hybridization. $|f_+\rangle$ and $|f_-\rangle$ are protected by opposite mirror eigenvalue. Since S and M_x commute, $S|f_-\rangle$ has the mirror eigenvalue -1, preventing it from hybridizing with $|f_+\rangle$. Therefore, the four states are capable to produce a fourfold degenerate point in the ($k_x = 0,\ k_z = \pi$) high symmetry line [see Fig. 1(b)].

The accidental band crossing mechanism guarantees that the fourfold degenerate point is stable in a wide range of the parameter space[38] as long as the symmetries M_x, T, and S_z preserve. Unlike Dirac points which are isolated gap-closing points, the fourfold degenerate point serves as the crossing point of multiple nodal rings. Specifically, three kinds of nodal rings each between two adjacent bands are presented in wurtzite GaN, which will be verified by calculation in Sec. IV, as shown in Fig. 1(c). All intersecting nodal rings are in the mirror plane $k_x = 0$, thus named the planar nodal chain.

The discussion above can be generalized to space groups in which the three symmetries M_α, S_β, and T are present, where α and β are two nonparallel directions, denoting the mirror plane direction and the screw axis, respectively. Since the screw symmetry is non-symmorphic, the symmetry conditions only apply to non-symmorphic space groups. In addition, the mirror symmetry-protected nodal rings break down in the presence of spin–orbit coupling, so the symmetry conditions are not valid in electronic systems. Among all 230 space groups, we identified 8 candidates for the planar nodal chain phonons, as listed in Table I. Some realistic materials are also given, of which Si_2N_2O is a kind of ceramic, GaN and AlN are wide bandgap semiconductors, and NaS is used in sodium–sulfur batteries. In the following, we will take wurtzite GaN (space group No.186) as an example to illustrate the planar nodal chain phonons. Wurtzite GaN is widely used in high-power electronics due to its wide bandgap and high carrier density. Yet, their performance and lifetime are restricted by heat dissipation

TABLE I. The complete list of all space groups that can host planar nodal chains.

Bravais lattice	Space group number	Space group symbol	Generators	Typical material
Orthorhombic	26	$Pmc2_1$	$S_{2z},\ M_x$	CaF_2[a]
	36	$Cmc2_1$	$S_{2z},\ M_x$	Si_2N_2O
	63	Cmcm	$S_{2z},\ M_x$	CaSi[a]
	67	Cmme	$S_{2y},\ M_x$	FeSe[a]
Hexagonal	185	$P6_3cm$	$S_{2z},\ M_x$	Li_2PS_3[a]
	186	$P6_3mc$	$S_{2z},\ M_x$	GaN
	193	$P6_3/mcm$	$S_{2z},\ M_x$	$TiCl_3$[a]
	194	$P6_3/mmc$	$S_{2z},\ M_x$	NaS

[a]Unstable materials.

efficiency. The exploration of topological phonon states offers new opportunities for tuning phonon transport in GaN devices.

III. COMPUTATION DETAILS

The phonon spectrum of wurtzite GaN is studied using density functional theory (DFT). All DFT calculations are performed with the Vienna Ab initio Simulation Package (VASP).[39] Projective augmented wave pseudopotential[40] in Perdew–Burke–Ernzerhof[41] formalism is employed for the exchange-correlation functional. The Phonopy package[42] is used to construct phonon dynamical matrices and compute the phonon dispersion. Iterative Green's function method[43] as implemented in WannierTools[44] is adopted to obtain the phonon surface state spectrum.

Lattice constants of wurtzite GaN are optimized under constraints of symmetry first. The electronic self-consistent loops are stopped when the total free energy drop between successive steps is below 10^{-7} eV. The break condition of ionic relaxation is that the norms of all the forces are smaller than 10^{-3} eV/Å. After relaxation, density functional perturbation theory is performed on a $4 \times 4 \times 3$ supercell with a Γ-centered $4 \times 4 \times 3$ k mesh to extract the second-order force constants. The phonon dispersion on high symmetry paths and two planes of interest (the $k_x = 0$ plane and the $k_z = \pi$ plane) are computed. The absence of imaginary frequencies in the phonon spectrum indicates that the relaxed structure is dynamically stable. To examine the existence of surface states, the phonon local density of states (LDOS) is calculated by iterative Green's function, in which the surface Hamiltonian is taken as simple stacks of the bulk tight-binding Hamiltonian.

IV. RESULTS AND DISCUSSION

Wurtzite GaN belongs to space group No. 186 ($P6_3mc$). Its unit cell is shown in Fig. 2(a). There are four atoms in the unit cell and, thus, are 12 phonon branches. The optimized lattice constants are $a = 3:216$ Å and $c = 5:240$ Å. Figure 2(b) shows the first Brillouin zone of bulk GaN and the projected surface Brillouin zones on the [0001] surface and the [10(–1)0] surface. High symmetry points in bulk and surface Brillouin zones are labeled. The generators of space group No. 186 are mirror symmetry M_x, twofold screw symmetry S_{2z} and threefold rotation symmetry C_{3z}. As discussed above, the mirror symmetry M_x is capable to protect the nodal rings in the mirror-invariant plane Γ-A-L-M. The twofold screw symmetry S_{2z} and time-reversal symmetry T ensure Kramers degeneracy in the $k_z = \pi$ plane, i.e., the A-L-H plane, making it a nodal surface (NS) for all bands, which means every phonon band in the $k_z = \pi$ plane is twofold degenerate. M_x, S_{2z}, and T together generate a planar nodal chain in the Γ-A-L-M plane. Figure 2(c) displays the phonon dispersion of wurtzite GaN along high symmetry paths, along with the nodal plane A-L-H and the fourfold degenerate point D. Calculation results show the coordinate of the D point is (0:384, 0, 0:5) in reciprocal lattice units and the degenerate frequency at the D point is 4.93 THz.

To verify the existence of the nodal rings and the planar nodal chains, we thoroughly calculate the phonon dispersion in three dimensions in k space. The exact shape of the planar nodal chain is plotted in Fig. 3(a), which is similar to that in Fig. 1(c), that is,

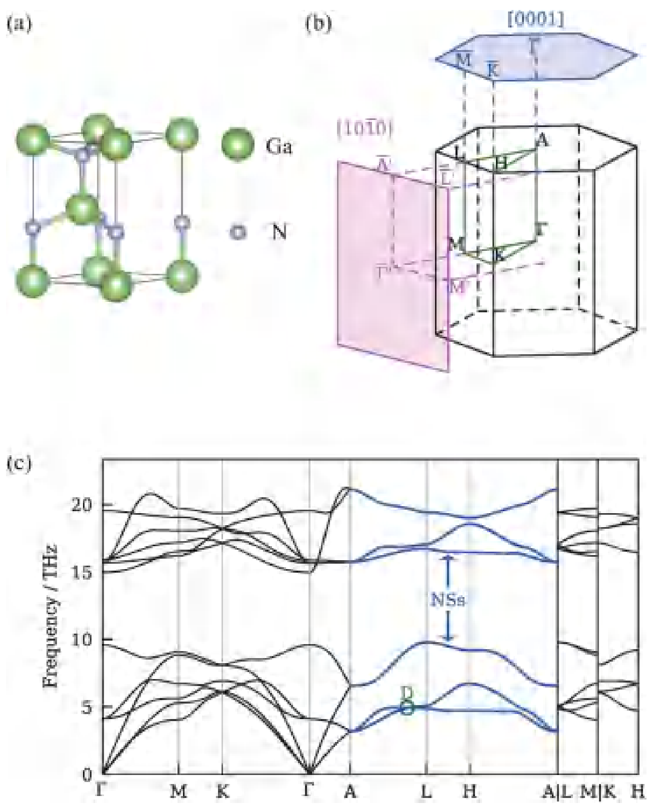

FIG. 2. (a) The lattice structure of wurtzite GaN. (b) First Brillouin zone of bulk GaN and its projection on the [0001] surface (blue) and the [10(−1)0] surface (magenta). (c) Phonon dispersions along high symmetry paths of wurtzite GaN. Nodal surface (NS) degeneracies are denoted by solid blue lines. The green circle marks the fourfold degenerate point, D.

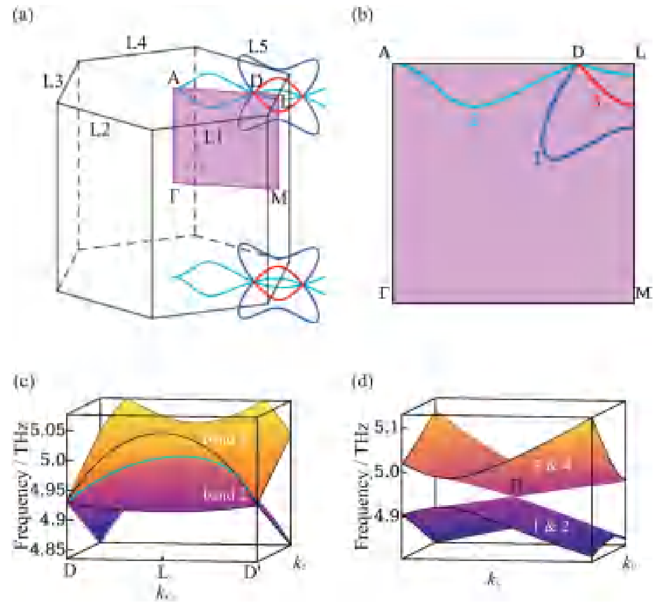

FIG. 3. (a) The planar nodal chains in k space. The red, blue, and cyan lines denote three kinds of nodal rings and D is their crossing point. For clarity, the planar nodal chains in five other directions (A-L1, A-L2, A-L3, A-L4, and A-L5) are not plotted, since they have the same shape due to sixfold screw symmetry. (b) The planar nodal chains plotted in the Γ-A-L-M plane. Numbers denote the occupation numbers of the nodal rings. For example, the cyan line is labeled 2, which means it is the degenerate line of the second and third bands. (c) Phonon dispersion of the second and third band in the $k_x = 0$ plane. The planar nodal chains formed by their crossing are represented by cyan lines. (d) Phonon dispersion near the D point in the $k_z = \pi$ plane. The first and second branches are degenerate. The third and fourth branches are degenerate. D is an isolated fourfold degenerate point in this plane.

three kinds of nodal rings intersect at the D point. Although not shown, there are also planar nodal chains in five other directions due to sixfold screw symmetry, which is a combination of twofold screw symmetry and threefold rotational symmetry. The blue lines are the degenerate lines of the first and second bands, the cyan ones are of the second and third bands, and the red ones are of the third and fourth bands, as shown in Fig. 3(b). Taking the cyan nodal ring as an example, Fig. 3(c) shows the phonon dispersion in the $k_x - k_z$ plane near D-L-D', proving the cyan nodal ring formed by the crossing of the second and third bands. Viewed in the $k_x = 0$ plane, D is the intersecting point of nodal rings, while viewed in the $k_z = \pi$ plane, D is an isolated band touching point that looks like the Dirac point in graphene,[45] as shown in Fig. 3(d).

To further confirm that the fourfold degenerate states are $|f_+\rangle$, $|f_-\rangle$, $S|f_+\rangle$, and $S|f_-\rangle$ as discussed in our theory, we examine the eigenvectors of phonons, i.e., the atom vibration directions. Mirror eigenvalue +1 means the state is mapped to itself by the mirror symmetry, so the atoms must vibrate in the $x = 0$ plane. Conversely, mirror eigenvalue −1 corresponds to atoms vibrating out of the $x = 0$ plane. The atom vibration directions of four degenerate bands at the D point are found to be two in-planes and two out-of-planes, verifying our prediction.

Next, we calculate the Berry phase γ along a closed path encircling the nodal ring,

$$\gamma = i\oint \sum_{n \in \mathrm{occ.}} \left\langle u_{n,k} \left| \frac{\partial}{\partial k} \right| u_{n,k} \right\rangle dk. \qquad (4)$$

The summation is done on occupied bands. All nodal rings have a Berry phase of π, indicating linear dispersion in the neighborhood of nodal rings.[23] Note that when both inversion and time-reversal symmetry are preserved, the Berry phase along any closed path is a multiple of π, so the integration path can arbitrarily deform as long as the gap is not closed. While in the case of wurtzite GaN where inversion symmetry is broken, the integration path is chosen close enough to the nodal ring to get a nearly-quantized Berry phase.

Nodal rings are accompanied by drumhead surface states on the surface.[32] In the presence of chiral symmetry, drumhead states are limited to the same energy, leading to surface superconductivity.[46] In phonon systems without chiral symmetry, the flatness of drumhead surface states is coincidental, depending on the surface roughness. We found drumhead surface states on two distinct surfaces, i.e., the [10(−1)0] surface and the [0001] surface. The phonon local density of states (LDOS) on the [10(−1)0] surface is shown in Fig. 4(a). The path is chosen as $\bar{A}$-$\bar{L}$-$\bar{A}$. The projection of the D point corresponds to the cone-shaped LDOS, verifying the semimetal-like point formed by band inversion. Drumhead surface states emanate from $\bar{D}$ in both directions, while those of a single nodal ring only spread in one direction of the nodal ring. The number of surface state branches also multiplies since D belongs to three nodal rings simultaneously. This further increases the surface density of states at $\bar{D}$ and benefits experimental verification. However, the drumhead states are not flat in energy due to the lack of chiral symmetry.

It is worth noting that previously reported nodal links or nodal chains are located on orthogonal mirror-symmetric planes, in both electrons[14] and phonons.[47] Drumhead surface states, emerging with nodal rings, are bounded by the projection of nodal rings on the surface Brillouin zone. However, mirror planes in wurtzite GaN are rotational-symmetric, which enables us to find a surface that is perpendicular to all mirror planes, i.e., the [0001] surface. The projections of mirror planes are one-dimensional lines on the [0001] surface. The projections of nodal rings are discrete line segments. However, thanks to the intersection of nodal rings, segments from different mirror planes [the cyan lines in Fig. 3(a)] still form a net on the [0001] surface Brillouin zone. Surface arc states connecting the nodal net on this surface are found, as shown in Fig. 4(c). Moreover, the connection is valid in a wide region in k space. We choose two paths, D-D' and E-E', shown in Fig. 4(b), where D is (0:384, 0) and E is (0:3, 0) in reciprocal lattice units. The phonon surface LDOS along them exhibits robust surface states, as shown in Figs. 4(d)–4(e).

The shape of the planar nodal chains in wurtzite GaN can be abstracted into multiple intersecting rings, as shown in Fig. 5(d), although they are not perfect circles in the realistic phonon spectrum. This simplified description can be generalized to other candidate space groups, where the planar nodal chains lie in the mirror-invariant plane, as plotted in Figs. 5(a)–5(c). Note that space groups 36, 63, and 67 all have the base-centered orthorhombic Bravais lattice, so they share the same first Brillouin zone shape. The same applies to space groups 185, 186, 193, and 194, which share the hexagonal Bravais lattice. In addition, the screw symmetry in space group 67 is S_y, while that in other candidate space groups is S_z, resulting in the difference in the direction of the planar nodal chains, as shown in Figs. 5(b) and 5(c).

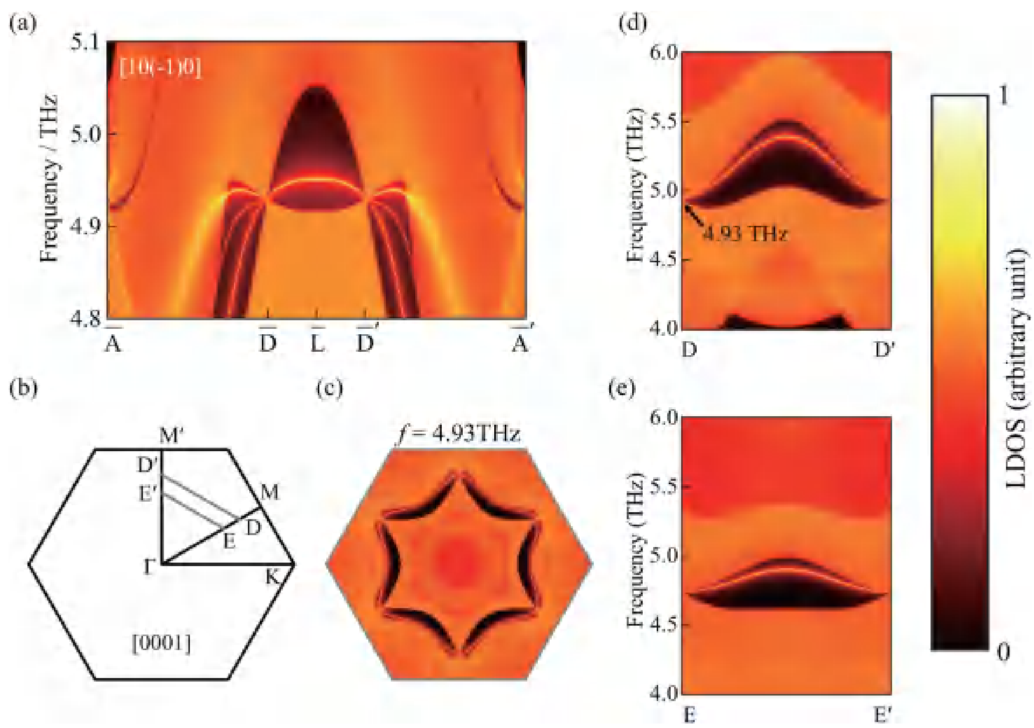

FIG. 4. (a) Phonon local density of states on the [10(−1)0] surface of wurtzite GaN along the $\bar{A}$-$\bar{L}$-$\bar{A}'$ path. Surface states emanating from the surface projection of D points are visible. (b). The [0001] surface Brillouin zone along with two k-paths, D-D′ and E-E′. (c) Iso-frequency surface at 4.93 THz on the [0001] surface Brillouin zone. (d) and (e) Phonon local density of states along D-D′ and E-E′, proving that the surface state is valid in a wide region in k space.

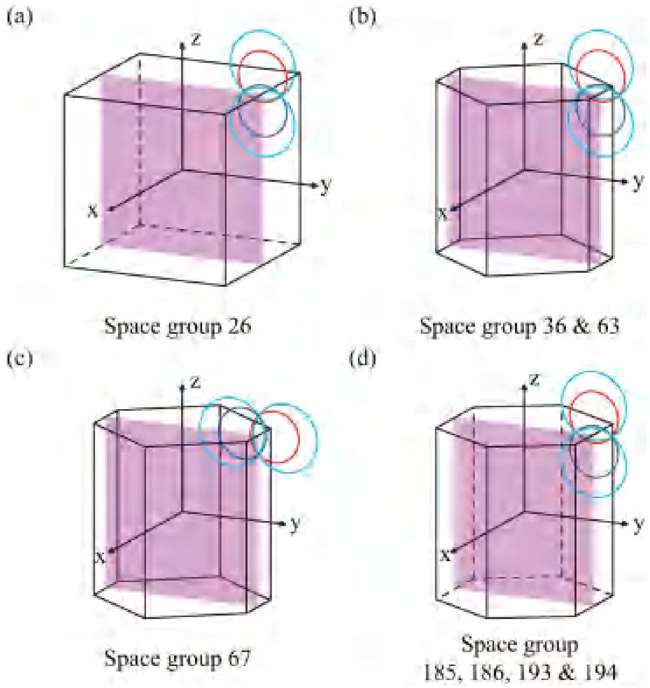

FIG. 5. Schematic diagrams for the planar nodal chains in eight candidate space groups. (a) Space group 26. (b) Space groups 36 and 63. (c) Space group 67. (d) Space groups 185, 186, 193, and 194. The magenta planes denote mirror-invariant planes in which the planar nodal chains lie. The red, blue, and cyan circles indicate the nodal rings that build up the planar nodal chains. For clarity, only one situation of the planar nodal chain is plotted in each subfigure.

V. CONCLUSIONS

In summary, we first identified a class of symmetry-enforced planar nodal chains in non-symmorphic phononic systems. The symmetry constraints of the planar nodal chain include mirror symmetry M_x, time-reversal symmetry T, and non-symmorphic screw symmetry S_{2z}. We identified 8 out of 230 space groups with proper symmetries to host the planar nodal chain. Using wurtzite GaN as an example, we illustrate the nodal chain phonons in detail based on first-principles calculations. Phonon surface density of states is calculated on the [10(–1)0] and the [0001] surface using iterative Green's function method. The former is inclined to the mirror plane while the latter is perpendicular to the mirror plane. Drumhead surface states are found inside the nodal ring, outside the nodal ring, and connecting different nodal rings. Our study reveals a class of symmetry-enforced planar nodal chain phonons in non-symmorphic materials and expands the catalog of topological nodal chains and related surface states.

ACKNOWLEDGMENTS

This work was supported by the National Natural Science Foundation of China (NNSFC) (Nos. 51825601 and U20A20301).

AUTHOR DECLARATIONS

Conflict of Interest

The authors have no conflicts to disclose.

Author Contributions

Hong-Ao Yang: Conceptualization (equal); Investigation (equal); Methodology (equal); Software (equal); Visualization (equal); Writing – original draft (equal). Hao-Yu Wei: Investigation (equal); Methodology (equal); Validation (equal); Writing – review & editing (equal). Bing-Yang Cao: Funding acquisition (equal); Project administration (equal); Supervision (equal); Writing – review & editing (equal).

DATA AVAILABILITY

The data that support the findings of this study are available from the corresponding author upon reasonable request.

REFERENCES

[1]A. Bansil, H. Lin, and T. Das, Rev. Mod. Phys. 88, 021004 (2016).
[2]F. D. M. Haldane, Rev. Mod. Phys. 89, 040502 (2017).
[3]X.-L. Qi and S.-C. Zhang, Rev. Mod. Phys. 83, 1057 (2011).
[4]N. P. Armitage, E. J. Mele, and A. Vishwanath, Rev. Mod. Phys. 90, 015001 (2018).
[5]C. Fu, Y. Sun, and C. Felser, APL Mater. 8, 040913 (2020).
[6]Z. Wang, Y. Sun, X.-Q. Chen, C. Franchini, G. Xu, H. Weng, X. Dai, and Z. Fang, Phys. Rev. B 85, 195320 (2012).
[7]Z. K. Liu, B. Zhou, Y. Zhang, Z. J. Wang, H. M. Weng, D. Prabhakaran, S.-K. Mo, Z. X. Shen, Z. Fang, X. Dai, Z. Hussain, and Y. L. Chen, Science 343, 864, (2014).
[8]H. Weng, C. Fang, Z. Fang, B. A. Bernevig, and X. Dai, Phys. Rev. X 5, 011029 (2015).
[9]B. Q. Lv, T. Qian, and H. Ding, Rev. Mod. Phys. 93, 025002 (2021).
[10]C. Fang, Y. Chen, H.-Y. Kee, and L. Fu, Phys. Rev. B 92, 081201 (2015).
[11]H. Weng, Y. Liang, Q. Xu, R. Yu, Z. Fang, X. Dai, and Y. Kawazoe, Phys. Rev. B 92, 045108 (2015).
[12]L. S. Xie, L. M. Schoop, E. M. Seibel, Q. D. Gibson, W. Xie, and R. J. Cava, APL Mater. 3, 083602 (2015).
[13]Y. Xu, Y. Gu, T. Zhang, C. Fang, Z. Fang, X.-L. Sheng, and H. Weng, APL Mater. 7, 101109 (2019).
[14]T. Bzdušek, Q. Wu, A. Rüegg, M. Sigrist, and A. A. Soluyanov, Nature 538, 75 (2016).
[15]R. Bi, Z. Yan, L. Lu, and Z. Wang, Phys. Rev. B 96, 201305 (2017).
[16]Q.-F. Liang, J. Zhou, R. Yu, Z. Wang, and H. Weng, Phys. Rev. B 93, 085427 (2016).
[17]W. Wu, Y. Liu, S. Li, C. Zhong, Z.-M. Yu, X.-L. Sheng, Y. X. Zhao, and S. A. Yang, Phys. Rev. B 97, 115125 (2018).
[18]T. Zhang, Z. Song, A. Alexandradinata, H. Weng, C. Fang, L. Lu, and Z. Fang, Phys. Rev. Lett. 120, 016401 (2018).
[19]J. Li, Q. Xie, S. Ullah, R. Li, H. Ma, D. Li, Y. Li, and X.-Q. Chen, Phys. Rev. B 97, 054305 (2018).
[20]D.-S. Tang and B.-Y. Cao, J. Appl. Phys. 129, 085102 (2021).
[21]T. T. Zhang, H. Miao, Q. Wang, J. Q. Lin, Y. Cao, G. Fabbris, A. H. Said, X. Liu, H. C. Lei, Z. Fang, H. M. Weng, and M. P. M. Dean, Phys. Rev. Lett. 123, 245302 (2019).
[22]J. Li, Q. Xie, J. Liu, R. Li, M. Liu, L. Wang, D. Li, Y. Li, and X.-Q. Chen, Phys. Rev. B 101, 024301 (2020).
[23]G. Liu, Y. Jin, Z. Chen, and H. Xu, Phys. Rev. B 104, 024304 (2021).

[24]R. Y. Wang, Z. J. Chen, Z. Q. Huang, B. W. Xia, and H. Xu, Phys. Rev. Mater. 5, 084202 (2021).
[25]Z. J. Chen, Z. J. Xie, Y. J. Jin, G. Liu, and H. Xu, Phys. Rev. Mater. 6, 034202 (2022).
[26]J. Wang, H. Yuan, Z.-M. Yu, Z. Zhang, and X. Wang, Phys. Rev. Mater. 5, 124203 (2021).
[27]X. Wang, F. Zhou, T. Yang, M. Kuang, Z.-M. Yu, and G. Zhang, Phys. Rev. B 104, L041104 (2021).
[28]J. Wang, H. Yuan, M. Kuang, T. Yang, Z.-M. Yu, Z. Zhang, and X. Wang, Phys. Rev. B 104, L041107 (2021).
[29]Q.-B. Liu, Z.-Q. Wang, and H.-H. Fu, Phys. Rev. B 104, L041405 (2021).
[30]Y. S. Chen, F. F. Huang, P. Zhou, Z. S. Ma, and L. Z. Sun, New J. Phys. 23, 103043 (2021).
[31]F. Zhou, Z. Zhang, H. Chen, M. Kuang, T. Yang, and X. Wang, Phys. Rev. B 104, 174108 (2021).
[32]J. Zhu, W. Wu, J. Zhao, H. Chen, L. Zhang, and S. A. Yang, npj Quantum Mater. 7, 1 (2022).
[33]H. Miao, T. T. Zhang, L. Wang, D. Meyers, A. H. Said, Y. L. Wang, Y. G. Shi, H. M. Weng, Z. Fang, and M. P. M. Dean, Phys. Rev. Lett. 121, 035302 (2018).
[34]J.-W. Jiang, B.-S. Wang, and H. S. Park, Nanoscale 10, 13913 (2018).
[35]R. Süsstrunk and S. D. Huber, Science 349, 47, (2015).
[36]C. He, X. Ni, H. Ge, X.-C. Sun, Y.-B. Chen, M.-H. Lu, X.-P. Liu, and Y.-F. Chen, Nat. Phys. 12, 1124 (2016).
[37]H. Pirie, S. Sadhuka, J. Wang, R. Andrei, and J. E. Hoffman, Phys. Rev. Lett. 128, 015501 (2022).
[38]B.-J. Yang and N. Nagaosa, Nat. Commun. 5, 4898 (2014).
[39]G. Kresse and J. Furthmüller, Phys. Rev. B 54, 11169 (1996).
[40]G. Kresse and D. Joubert, Phys. Rev. B 59, 1758 (1999).
[41]J. P. Perdew, K. Burke, and M. Ernzerhof, Phys. Rev. Lett. 77, 3865 (1996).
[42]A. Togo and I. Tanaka, Scr. Mater. 108, 1 (2015).
[43]M. P. L. Sancho, J. M. L. Sancho, J. M. L. Sancho, and J. Rubio, J. Phys. F: Metal Phys. 15, 851 (1985).
[44]Q. Wu, S. Zhang, H.-F. Song, M. Troyer, and A. A. Soluyanov, Comput. Phys. Commun. 224, 405 (2018).
[45]A. H. Castro Neto, F. Guinea, N. M. R. Peres, K. S. Novoselov, and A. K. Geim, Rev. Mod. Phys. 81, 109 (2009).
[46]Y. Chen, Y.-M. Lu, and H.-Y. Kee, Nat. Commun. 6, 6593 (2015).
[47]Y. J. Jin, Z. J. Chen, B. W. Xia, Y. J. Zhao, R. Wang, and H. Xu, Phys. Rev. B 98, 220103 (2018).